Search for axion-like dark matter with ferromagnets

Alexander V. Gramolin¹, Deniz Aybas^{1,2}, Dorian Johnson¹, Janos Adam¹, Alexander O. Sushkov^{1,2,3*}

¹Department of Physics, Boston University, Boston, MA 02215, USA ²Department of Electrical and Computer Engineering, Boston University, Boston, MA 02215, USA

³Photonics Center, Boston University, Boston, MA 02215, USA *To whom correspondence should be addressed; e-mail: asu@bu.edu

Abstract

Ultralight axion-like particles are well-motivated dark matter candidates, emerging naturally from theories of physics at ultrahigh energies. Here we report the results of a direct search for the electromagnetic interaction of axion-like dark matter in the mass range that spans three decades from 12 peV to 12 neV. The detection scheme is based on a modification of Maxwell's equations in the presence of axionlike dark matter, which mixes with a static magnetic field to produce an oscillating magnetic field. The experiment makes use of toroidal magnets with iron-nickel alloy ferromagnetic powder cores, which enhance the static magnetic field by a factor of 24. Using SQUIDs, we achieve a magnetic sensitivity of 150 aT/ $\sqrt{\text{Hz}}$, at the level of the most sensitive magnetic field measurements demonstrated with any broadband sensor. We recorded 41 hours of data and improved the best limits on the magnitude of the axion-like dark matter electromagnetic coupling constant over part of our mass range, at 20 peV reaching 4.0×10^{-11} GeV⁻¹ (95% confidence level). Our measurements are starting to explore the coupling strengths and masses of axionlike particles where mixing with photons could explain the anomalous transparency of the universe to TeV gamma-rays.

Astronomical evidence, built up over eight decades, indicates that only one-sixth of matter in the universe is made up of fundamental particles whose properties we understand [1, 2]. The existence of dark matter constitutes compelling evidence for new fundamental particles and interactions beyond the Standard Model. Since it has only

been observed through its gravitational effects, there is a broad range of dark matter candidates. The weakly-interacting massive particle (WIMP) is a candidate that has inspired a large number of ultra-sensitive experiments of increasing complexity and scale, but so far there has been no unambiguous detection, and fundamental backgrounds (neutrino floor) will soon start to limit the sensitivity of direct WIMP searches [3, 2, 4]. Another well-motivated dark matter candidate is the axion, which also offers a compelling solution to the strong CP problem of quantum chromodynamics [5, 6, 7, 8, 9, 10]. The axion and other light pseudoscalar bosons (axion-like particles, ALPs) emerge naturally from theoretical models of physics at high energies, including string theory, grand unified theories, and models with extra dimensions [11, 10]. Astrophysical observations have produced a number of stringent limits on ALPs [12, 13], but also some tantalizing hints for their possible existence [2]. One such hint is the observation that the universe is too transparent to TeV γ -rays. These are emitted from distant active galactic nuclei and should be significantly attenuated, through pair production, by infrared background radiation during their travel to our galaxy [14]. The tension with observed TeV gamma-ray source energy spectra can be explained by photon-ALP mixing inducing gamma-ray conversion into axions, which travel unaffected through interstellar space and convert back into gamma-rays in the Milky Way [15].

Experimental searches for the axion and ALPs rely on one of their interactions with Standard Model particles [16, 17, 18, 10, 19]. Most experiments to date have focused on the axion-photon interaction, which can mix photons with axions and ALPs in the presence of a strong magnetic field. The conversion rate scales with magnetic field and volume, so experiments employ large magnetic fields and volumes for better sensitivity [20]. This effect has been used to place stringent limits on the coupling of ALPs produced in the laboratory [21], or in the Sun [22]. Several searches for axion dark matter in the μ eV

mass range have used the technique of resonant conversion into monochromatic microwave photons inside a high-quality-factor cavity permeated by a strong magnetic field [23]. The ADMX experiment has achieved a level of sensitivity sufficient to search for dark matter axions with masses between 2.66 and 2.81 μ eV and excluded the QCD axion-photon couplings predicted by plausible models for this mass range [24]. A number of cavity-based axion dark matter searches are in development or already exploring ALP masses up to $\approx 30~\mu$ eV [23, 25, 26, 27, 28, 29, 30]. In order to search for lower-mass axions and ALPs coupled to photons, it is possible to use lumped-element circuits [31, 32, 33, 34, 35]. This concept is based on a modification of Maxwell's equations: in the presence of a large static magnetic field B, axion-like dark matter acts as a source of an oscillating magnetic field whose amplitude is proportional to B [36, 37].

Our approach is to use a toroidally-shaped permeable material to enhance the magnitude of the static magnetic field B and thus improve sensitivity to axion-like dark matter. In the presence of a magnetizable medium, the modified inhomogeneous magnetic Maxwell's equation takes the form

$$\vec{\nabla} \times \vec{H} = \vec{J}_f + \frac{g_{a\gamma}}{\mu_0 c} \frac{\partial a}{\partial t} \vec{B}, \tag{1}$$

where $\vec{H} = \vec{B}/\mu_0 - \vec{M}$ is the auxiliary field, \vec{M} is the magnetization, \vec{J}_f is the macroscopic free electric current density, μ_0 is the permeability of free space, c is the speed of light in vacuum, and $g_{a\gamma}$ is the strength of ALP electromagnetic coupling (Supplementary Information). The axion-like dark matter field $a = a_0 \sin{(\omega_a t)}$ oscillates at its Compton frequency $\nu_a = \omega_a/(2\pi) = m_a c^2/h$, where m_a is the ALP mass, and h is the Planck constant. The coherence time of this oscillating field is $\approx 10^6$ periods, set by the kinetic energy of the virialized axionic dark matter [36, 16]. We use SI units for electromagnetic fields and natural units for the ALP field so that $g_{a\gamma}a_0$ is unitless, and the ALP field amplitude a_0

is given by the dark matter energy density: $m_a^2 a_0^2/2 = \rho_{\rm DM} = 3.6 \times 10^{-42} \text{ GeV}^4$ [2, 16].

Our experiment, the Search for Halo Axions with Ferromagnetic Toroids (SHAFT), contained two independent detection channels. Each channel consisted of two stacked toroids, each of which could be independently magnetized by injecting a current into a superconducting magnetizing coil wound around the toroid, fig. 1(a). With azimuthal field B_0 inside the magnetized toroid, the second term in the right-hand side of eq. (1) represents an effective current density, $J_{\text{eff}} = \omega_a g_{a\gamma} a_0 \cos(\omega_a t) B_0/(\mu_0 c)$, sourced by the axion-like dark matter field. This loop of current creates an axial magnetic field B_a . The pickup coil, wound around the inner circumference of the toroids, was coupled to a Superconducting Quantum Interference Device (SQUID) magnetometer, as shown in fig. 1(b), measuring the magnetic flux Φ_a due to B_a . The axion-like dark matter detection signature would be an oscillating SQUID output signal, whose amplitude was correlated with toroid magnetization.

The two-channel, four-toroid design enabled a systematic rejection scheme that allowed for discrimination between an axion-like dark matter signal and electromagnetic interference, fig. 1(c). For collecting data sensitive to axion-like dark matter, we magnetized the top two toroids counter-clockwise (channel A: ++), and the bottom two toroids clockwise (channel B: --), viewed from the top. An axion-like dark matter signal would then appear in the two detector channels with opposite sign (180° out of phase). Electromagnetic interference, uncorrelated with toroid magnetization, would not have such a phase relationship and could be distinguished from an axion-like dark matter signal by forming symmetric and antisymmetric combinations of the two detector channels. The toroids and pickup coils were inside an enclosure formed by two nested coaxial cylinders immersed in liquid helium. Lead foil, affixed to the inner surfaces of the cylinders and their caps, formed a double-layer superconducting magnetic shield, suppressing electro-

magnetic interference and ambient magnetic field noise.

The sensitivity enhancement in our approach arises from the fact that the magnetic field inside the permeable toroids includes material magnetization in addition to the field created by the free current in the toroidal magnetizing coil: $\vec{B}_0 = \mu_0(\vec{H}_0 + \vec{M}_0)$. For a linear magnetic material with permeability μ , $B_0 = \mu \mu_0 H_0$ and the magnetic field enhancement is by a factor equal to μ . In practice, magnetic materials are non-linear: the incremental permeability drops with applied field H_0 and the magnetization saturates. For our experiment, we chose powdered iron-nickel "High Flux 125μ " alloy for its high permeability, high saturation flux density, and electrical insulating properties at liquid helium temperature (Supplementary Information). We determined the incremental permeability of the toroid material by injecting currents up to 10 A into the magnetizing coil and measuring its inductance. The initial permeability was ≈ 110 , dropping with increasing coil current as the material saturated, fig. 2(a). The material displayed no magnetic hysteresis. We used the incremental permeability measurements to calculate magnetic field B_0 inside the toroid at each value of the magnetizing coil current using $B_0(H_0) = \mu_0 \int_0^{H_0} \mu(H) dH$, fig. 2(b). Before recording data sensitive to ALP dark matter, we set the magnetizing coil current to 6 A, at which point $B_0 = 1.51$ T and the material is close to saturation. At this current, the magnetic field inside an air-core toroid would be 0.063 T (dashed red line in fig. 2(b)). Therefore, we can quantify the enhancement of B_0 due to the magnetic material to be a factor of 24. During ALP-sensitive data collection, we switched each of the magnetizing coils into persistent mode, but still monitored each toroid magnetization by making inductance measurements of separate permeability sensing coils, which had been calibrated in advance (Supplementary Information).

Quantifying the sensitivity of our experiment to an axion-like dark matter signal required measurements of the magnetic field sensitivity of the two detection channels. The

experimental design included four independent single-turn calibration loops, mounted at several positions near the toroids (Supplementary Information). We performed calibration measurements by injecting sinusoidally-varying current with known frequency and amplitude into each loop and recording the response of both SQUID channels. Measurements with the central calibration loop, which was positioned midway between the upper and the lower toroid pairs, and thus had equal couplings to the two pickup coils, showed that the detector channels were in phase, fig. 3(a). We recorded the SQUID output $V_{\rm SQ}$ for a range of calibration current frequencies and used the numerically-computed mutual inductance to calculate the magnetic flux Φ through each pickup coil. These measurements established the calibration of the flux-to-voltage transfer function $x = V_{\rm SQ}/\Phi$, whose magnitude was consistent with the inductive coupling model shown in fig. 1(b), and whose frequency dependence was consistent with a second-order low-pass filter model, fig. 3(b). The transfer function measurements for all calibration loops mounted inside the experiment were consistent within a 25% range (Supplementary Information).

The main factor limiting the sensitivity of our ALP dark matter search was SQUID sensor noise. To quantify magnetic sensitivity, we magnetized the toroids with 6 A injected current, recorded the SQUID output voltage, converted it to magnetic field using the transfer function for each SQUID detector channel, and calculated the Fourier spectra, fig. 3(c,d). Below 3 kHz, the spectra were dominated by vibrations of the pickup coil in the magnetic field leaking out of the magnetized toroids, and above 3 MHz, the sensitivity was degraded by the SQUID feedback electronics bandwidth roll-off. Aside from several noise peaks due to residual radiofrequency (RF) interference, between 10 kHz and 1 MHz the noise spectrum was very nearly flat at the level of 150 aT/ $\sqrt{\text{Hz}}$. This is at the level of the most sensitive magnetic field measurements demonstrated with broadband SQUID systems [38] or atomic magnetometers [39], in spite of the direct proximity of

ferromagnetic material magnetized to 1.51 T. The absence of detectable magnetization noise from the ferromagnetic toroids was due to the pickup coil geometry, designed to be insensitive to toroid magnetization fluctuations [40, 41]. For our axion-like dark matter search, we chose the frequency range between 3 kHz and 3 MHz so that the noise was within a factor of 3 of the baseline.

The experimental run took place on September 12–17, 2019. After performing calibrations described above, we magnetized the four toroids with 6 A injected current in (++, --) configuration and recorded 41 hours of data that were used to search for axion-like dark matter signals. Afterwards, we magnetized the four toroids with 6 A injected current in (+-, +-) configuration and collected 15 hours of data. Since in each channel the toroid magnetizations were now opposite, the axion-induced flux would vanish and we could use these data to confirm or reject any potential detection extracted from the first data set. We also collected 12 hours of data with no toroid magnetization, for the same purpose. In each data run, output voltages from the two SQUID detector channels were digitized at the sampling rate of 15.625 MS/s and recorded to a hard disk drive. We used the permeability sensing coils to monitor each toroid magnetization, and ensured that all magnetizations were unchanged before and after recording each data set. We note that experimental sensitivity to $g_{a\gamma}$ has a slow 1/4-power scaling with averaging time, provided it exceeds ALP coherence time [17].

Data analysis consisted of several processing, correction, and axion-like dark matter signal search steps. We divided the data into blocks of duration 2199 s (2^{35} samples), chosen to be much longer than the ALP dark matter field coherence time for every frequency in the exclusion region. After removing 20 data blocks where SQUID feedback reset jumps occurred, we performed a discrete Fourier transform on each of the remaining 47 data blocks, used the SQUID detector transfer function x to convert the frequency-domain data

from voltage to magnetic flux Φ , and formed symmetric and antisymmetric combinations of the two detector channels: $\Phi_+ = (\Phi_A + \Phi_B)/2$ and $\Phi_- = (\Phi_A - \Phi_B)/2$. We calculated the power spectral density (PSD) for each of the four data streams $\Phi^2_{(A,B,+,-)}$, and averaged each PSD over all the blocks in the experimental run. We modeled each spectrum as the sum of an axion-like dark matter signal, SQUID detector noise, narrowband RF interference, and a broadband spectral baseline due to vibrational pickup of magnetic flux leakage from toroids. Our analysis assumed the boosted Maxwell-Boltzmann ALP signal lineshape predicted by the astrophysically-motivated standard halo model [42, 25, 43, 24]. The linewidth of an axion-like dark matter signal at frequency ν_a is determined by the parameter $\beta^2 \nu_a = 3v_0^2 \nu_a/(2c^2) \approx 10^{-6} \nu_a$, where $v_0 = 220$ km/s is the local velocity of motion around the center of the galaxy. Following a simplified version of the data analysis approach used by the ADMX and HAYSTAC collaborations, we rejected narrowband RF interference and broadband spectral baseline by using Savitzky-Golay digital filtering to isolate these spectral features in the frequency domain [43, 24]. By injecting simulated axion signals into the data, we determined that these corrections attenuated axion spectral signals by 7\%, and the final limits were adjusted accordingly (Supplementary Information).

We performed the search for axion-like signals independently in each of the averaged spectra $\langle \Phi^2_{(A,B,+,-)} \rangle$ in the frequency range from 3 kHz to 3 MHz. In this range, each spectrum contained 6.6×10^9 independent frequency points, which we broke up into 857 frequency bins, with bin width set to $10^4 \beta^2 \nu_b$, where ν_b is the bin center frequency. We modeled the histogram of PSD values in each bin as the chi-square distribution with 94 degrees of freedom, corresponding to the two quadratures of the Fourier transform averaged over 47 independent data blocks, fig. 4(a). We optimally filtered the data within each frequency bin by convolving with the standard halo model axion lineshape. We

modeled the histogram of optimally-filtered data points as the normal distribution (verified by a Lilliefors test), and found its standard deviation σ by fitting to the Gaussian dependence, fig. 4(b). We set the candidate detection threshold to 3.355σ , equivalent to 95% confidence interval for a 5σ detection [43], and flagged all points above the threshold as candidates. In the 3 kHz to 3 MHz frequency range, with our analysis parameters, there were 20 043 605 possible ALP frequency points. Assuming the optimally-filtered spectra are normally distributed, we would statistically expect 7954 candidate frequencies at which the spectral value is above the 3.355σ threshold in any given channel. Our analysis procedure produced 16 292 candidates in channel A, 35 375 candidates in channel B, 27 278 candidates in the symmetric combination channel, and 12 513 candidates in the antisymmetric combination channel. The extra candidates appeared due to residual electromagnetic interference and lower-frequency vibrational tones that got past our spectral correction procedure.

Resonant experiments, such as ADMX and HAYSTAC, perform re-scans of candidate frequencies to check if they are statistical deviations or a real axion signal. In our analysis, we used the two detector channels to make this decision. Axion-like dark matter detection claim would be made for candidates that are above threshold for the antisymmetric channel and in both channels A and B, but not in the symmetric channel. None of the candidates satisfied all four of these detection conditions. As a check of our data analysis procedure, we injected numerically-generated ALP signals into our data and verified that our analysis recovered the signals with their correct coupling strengths (Supplementary Information). We used the conversion $\Phi_a = \omega_a g_{a\gamma} a_0 B_0 V/c$ between the ALP electromagnetic coupling $g_{a\gamma}$ and the induced magnetic flux Φ_a through the pickup coil, with the the mean magnetic field $B_0 = (1.51 \pm 0.03)$ T at 6 A magnetizing current and the effective volume of each channel $V = (10.3 \pm 0.4)$ cm³. We calculated the effective volume numer-

ically, taking into account the $\approx 20\%$ suppression due to the Meissner effect in the lead superconducting magnetic shield (Supplementary Information).

In the absence of a detection, we report for each frequency bin the magnitude of $g_{a\gamma}$ corresponding to the 5σ value of the optimally-filtered magnetic flux PSD in the antisymmetric channel, which represents the 95% confidence interval limit for that bin, fig. 4(c). Before our work, the best experimental limit on the ALP-photon coupling for this mass range was set by the CERN CAST helioscope search for solar axions at $0.66 \times 10^{-10} \text{ GeV}^{-1}$ [22]. Despite the much smaller volume of our apparatus (by a factor of ≈ 300), our results constitute significant improvements on this limit over a broad range of ALP masses in the scenario that the ALP field is the dominant component of dark matter. Our experiment begins the exploration of the ALP mass and coupling region near $m_a \gtrsim 0.7$ neV and $g_{a\gamma} \lesssim 8.8 \times 10^{-10} \text{ GeV}^{-1}$, where existence of ALPs may resolve the tension between the observed TeV gamma-ray energy spectrum and the one expected based on the recent cosmic infrared background radiation data [15].

There are several ways to improve experimental sensitivity to axion-like dark matter. Cooling the SQUID magnetic sensors to milli-Kelvin temperature can reduce their noise by a factor of ≈ 10 , and it may be possible to achieve even better sensor performance using quantum upconversion [44]. For an optimized search, it is necessary to use a scanned single-pole resonator to couple the ALP-induced magnetic flux to an amplifier operating at, or beyond, the Standard Quantum Limit [45]. The ferromagnetic toroidal core allowed us to achieve a 1.51 T static magnetic field with ampere-level injected current, which enabled the two-channel design, but magnetic material saturation prevented further field increase. New magnetic materials, with higher saturation field, could improve sensitivity further, or a high-field air-core toroidal superconducting magnet could be engineered, needing much higher injected current [20]. The most dramatic sensitivity improvement

could be achieved by increasing the toroid volume; the Fe-Ni magnetic alloy used in our experiment is inexpensive and readily available commercially. Scaling the volume up to the benchmark 1 m^3 would improve the sensitivity by another factor of 10^4 .

Methods

Four "High Flux 125 μ " toroidal cores made of powdered Fe-Ni alloy were obtained from MH&W International Corporation (part number CH778125E). We refer to these toroids as A1 (uppermost), A2, B1, and B2 (lowermost). The cores have a rectangular cross-section and the following dimensions: inner radius $r_1 = 24.4$ mm, outer radius $r_2 = 39.1$ mm, and height h = 16.2 mm. A magnetizing coil was wound around each toroid using 0.006" diameter polyimide-insulated Nb 48% Ti wire obtained from California Fine Wire. Each magnetizing coil consisted of two counter-wound layers (to cancel out the azimuthal component of the current) with the following total number of turns: $N_m^{A1} = 1676$, $N_m^{A2} = 1678$, $N_m^{B1} = 1655$, and $N_m^{B2} = 1679$. In each detection channel, referred to as A (B), toroids A1 and A2 (B1 and B2) were stacked top-to-bottom. Within each channel, the two toroids could be independently magnetized in the same or the opposite directions by choosing polarities of currents in the magnetizing coils.

Nb-Ti twisted pairs and Nb washers were used to connect each magnetizing coil to a persistent switch placed within the outer superconducting shield. Each persistent switch consisted of a section of Nb-Ti wire encapsulated in Stycast 2850FT epoxy together with a 50 Ω surface-mount resistor (a persistent switch heater); applying a current pulse to the resistor made the Nb-Ti wire go from superconducting to normal and opened the persistent switch.

The same Nb-Ti wire was used to wind two SQUID pickup coils (with 6 turns each) on the G-10 support rod, on which the toroids were mounted using Stycast 2850FT epoxy. Each pickup coil was connected to a Magnicon single-stage SQUID sensor using a twisted pair. During data collection, the SQUIDs were operated in a flux-locked-loop (FLL) mode with the amplifier feedback resistance $R_f = 30 \text{ k}\Omega$ and the gain-bandwidth product 7.20 GHz. Experimental calibration of the SQUID frequency response is described in Supplementary Information.

During data collection runs, we used a custom cryogenic relay to disconnect all the twisted pair leads (other than those of the pickup coils) entering the inner superconducting shield. This allowed us to reduce the RF interference signals entering the experiment. The cryogenic relay, placed within the outer superconducting shield, consisted of 50 individual reed switches manufactured by Standex Electronics (part number KSK-1A85-2030). These reed switches were placed inside a G-10 tube, which was filled with Stycast 2850FT epoxy. On the outer surface of the tube, a solenoidal coil was wound using copper magnet wire. By running a 2.5 A current through this coil, we could activate the reed switches, which were normally open. For the magnetizing coils, we used three reed switches connected in parallel (six switches in total per a twisted pair), which allowed us to achieve the carry current of 10 A at liquid-helium temperature.

When the toroids were magnetized, some fraction of the magnetic field leaked out and coupled into the pickup coils. In order to address the issue of seismic vibrations causing the pickup coils to move relative to this stray magnetic field, a tripod was constructed to support the cryostat housing the apparatus by connecting an aluminum frame to three Newport I-2000 high performance laminar flow isolators. Seismic isolation of the apparatus from the ground led to reduction of vibrational magnetic pickup at acoustic frequencies, which simplified the procedure of locking SQUID electronics feedback loops.

Acknowledgements: The authors thank Ben Brubaker for valuable discussions

about data analysis. The authors acknowledge support from the NSF grant 1806557,

the Heising-Simons Foundation grant 2015-039, the Simons Foundation grant 641332,

and the Alfred P. Sloan foundation grant FG-2016-6728.

Author contributions: A.O.S. conceived and supervised the research. A.V.G.,

A.O.S., and D.J. designed and built the experimental apparatus. D.A. developed the

data acquisition system. D.J. performed the COMSOL simulations. A.V.G. and J.A.

carried out the magnetic permeability measurements. A.O.S. and A.V.G. analyzed the

data. All authors contributed to data collection and writing the manuscript.

Competing interests: The authors declare no competing interests.

Data availability: Source data are available for this paper. All other data that

support the plots within this paper and other findings of this study are available from the

corresponding author upon reasonable request.

Code availability: The code that supports the plots within this paper are available

from the corresponding author upon reasonable request.

Supplementary Content:

Supplementary Text

Figures S1 to S6

Tables S1 to S6

14

References

- [1] Spergel, D. N. The dark side of cosmology: dark matter and dark energy. *Science* **347**, 1100–1102 (2015).
- [2] Tanabashi, M. et al. Review of particle physics. Phys. Rev. D 98, 030001 (2018).
- [3] Liu, J., Chen, X. & Ji, X. Current status of direct dark matter detection experiments.

 Nat. Phys. 13, 212–216 (2017).
- [4] Rajendran, S., Zobrist, N., Sushkov, A. O., Walsworth, R. & Lukin, M. A method for directional detection of dark matter using spectroscopy of crystal defects. *Phys. Rev. D* 96, 035009 (2017).
- [5] Preskill, J., Wise, M. B. & Wilczek, F. Cosmology of the invisible axion. *Phys. Lett.* B 120, 127–132 (1983).
- [6] Abbott, L. F. & Sikivie, P. A cosmological bound on the invisible axion. Phys. Lett. B 120, 133–136 (1983).
- [7] Dine, M. & Fischler, W. The not-so-harmless axion. *Phys. Lett. B* **120**, 137–141 (1983).
- [8] Arias, P. et al. WISPy cold dark matter. J. Cosmol. Astropart. Phys. 1206, 013 (2012).
- [9] DeMille, D., Doyle, J. M. & Sushkov, A. O. Probing the frontiers of particle physics with tabletop-scale experiments. *Science* **357**, 990–994 (2017).
- [10] Irastorza, I. G. & Redondo, J. New experimental approaches in the search for axionlike particles. Prog. Part. Nucl. Phys. 102, 89–159 (2018).

- [11] Svrcek, P. & Witten, E. Axions in string theory. J. High Energy Phys. 0606, 051 (2006).
- [12] Payez, A. et al. Revisiting the SN1987A gamma-ray limit on ultralight axion-like particles. J. Cosmol. Astropart. Phys. 1502, 006 (2015).
- [13] Chang, J. H., Essig, R. & McDermott, S. D. Supernova 1987A constraints on sub-GeV dark sectors, millicharged particles, the QCD axion, and an axion-like particle. J. High Energy Phys. 1809, 051 (2018).
- [14] Matsuura, S. et al. New spectral evidence of an unaccounted component of the near-infrared extragalactic background light from the CIBER. Astrophys. J. 839, 7 (2017).
- [15] Kohri, K. & Kodama, H. Axion-like particles and recent observations of the cosmic infrared background radiation. Phys. Rev. D 96, 051701 (2017).
- [16] Graham, P. W. & Rajendran, S. New observables for direct detection of axion dark matter. Phys. Rev. D 88, 035023 (2013).
- [17] Budker, D., Graham, P. W., Ledbetter, M., Rajendran, S. & Sushkov, A. O. Proposal for a cosmic axion spin precession experiment (CASPEr). *Phys. Rev. X* 4, 021030 (2014).
- [18] Arvanitaki, A. & Geraci, A. A. Resonantly detecting axion-mediated forces with nuclear magnetic resonance. *Phys. Rev. Lett.* **113**, 161801 (2014).
- [19] Crescini, N. et al. Axion search with a quantum-limited ferromagnetic haloscope. *Phys. Rev. Lett.* **124**, 171801 (2020).
- [20] Battesti, R. et al. High magnetic fields for fundamental physics. Phys. Rep. 765–766, 1–39 (2018).

- [21] Ehret, K. et al. New ALPS results on hidden-sector lightweights. *Phys. Lett. B* **689**, 149–155 (2010).
- [22] Anastassopoulos, V. et al. New CAST limit on the axion-photon interaction. *Nat. Phys.* **13**, 584–590 (2017).
- [23] Graham, P. W., Irastorza, I. G., Lamoreaux, S. K., Lindner, A. & van Bibber, K. A. Experimental searches for the axion and axion-like particles. Ann. Rev. Nucl. Part. Sci. 65, 485–514 (2015).
- [24] Du, N. et al. Search for invisible axion dark matter with the axion dark matter experiment. *Phys. Rev. Lett.* **120**, 151301 (2018).
- [25] Brubaker, B. M. et al. First results from a microwave cavity axion search at 24 μ eV. *Phys. Rev. Lett.* **118**, 061302 (2017).
- [26] McAllister, B. T. et al. The ORGAN experiment: an axion haloscope above 15 GHz. Phys. Dark Univ. 18, 67–72 (2017).
- [27] Melcón, A. Á. et al. Axion searches with microwave filters: the RADES project. *J. Cosmol. Astropart. Phys.* **1805**, 040 (2018).
- [28] Alesini, D. et al. KLASH conceptual design report. Preprint at https://arxiv.org/ abs/1911.02427 (2019).
- [29] Alesini, D. et al. Galactic axions search with a superconducting resonant cavity. *Phys. Rev. D* **99**, 101101 (2019).
- [30] Lee, S., Ahn, S., Choi, J., Ko, B. R. & Semertzidis, Y. K. Axion dark matter search around 6.7 μ eV. Phys. Rev. Lett. **124**, 101802 (2020).

- [31] Sikivie, P., Sullivan, N. & Tanner, D. B. Proposal for axion dark matter detection using an *LC* circuit. *Phys. Rev. Lett.* **112**, 131301 (2014).
- [32] Chaudhuri, S. et al. Radio for hidden-photon dark matter detection. *Phys. Rev. D* **92**, 075012 (2015).
- [33] Kahn, Y., Safdi, B. R. & Thaler, J. Broadband and resonant approaches to axion dark matter detection. *Phys. Rev. Lett.* **117**, 141801 (2016).
- [34] Chaudhuri, S., Irwin, K., Graham, P. W. & Mardon, J. Fundamental limits of electromagnetic axion and hidden-photon dark matter searches: part I the quantum limit. Preprint at https://arxiv.org/abs/1803.01627 (2018).
- [35] Ouellet, J. L. et al. First results from ABRACADABRA-10 cm: a search for sub- μ eV axion dark matter. *Phys. Rev. Lett.* **122**, 121802 (2019).
- [36] Sikivie, P. Experimental tests of the "invisible" axion. *Phys. Rev. Lett.* **51**, 1415–1417 (1983).
- [37] Wilczek, F. Two applications of axion electrodynamics. *Phys. Rev. Lett.* **58**, 1799–1802 (1987).
- [38] Storm, J.-H., Hömmen, P., Drung, D. & Körber, R. An ultra-sensitive and wideband magnetometer based on a superconducting quantum interference device. Appl. Phys. Lett. 110, 072603 (2017).
- [39] Dang, H. B., Maloof, A. C. & Romalis, M. V. Ultrahigh sensitivity magnetic field and magnetization measurements with an atomic magnetometer. *Appl. Phys. Lett.* 97, 151110 (2010).

- [40] Eckel, S., Sushkov, A. O. & Lamoreaux, S. K. Magnetic susceptibility and magnetization fluctuation measurements of mixed gadolinium-yttrium iron garnets. *Phys. Rev. B* 79, 014422 (2009).
- [41] Sushkov, A. O., Eckel, S. & Lamoreaux, S. K. Prospects for a new search for the electron electric-dipole moment in solid gadolinium-iron-garnet ceramics. *Phys. Rev.* A 79, 022118 (2009).
- [42] Turner, M. S. Periodic signatures for the detection of cosmic axions. *Phys. Rev. D* 42, 3572–3575 (1990).
- [43] Brubaker, B. M., Zhong, L., Lamoreaux, S. K., Lehnert, K. W. & van Bibber, K. A. HAYSTAC axion search analysis procedure. *Phys. Rev. D* **96**, 123008 (2017).
- [44] Chaudhuri, S. The Dark Matter Radio: a Quantum-Enhanced Search for QCD Axion Dark Matter. PhD thesis, Stanford Univ. (2019).
- [45] Chaudhuri, S., Irwin, K. D., Graham, P. W. & Mardon, J. Optimal electromagnetic searches for axion and hidden-photon dark matter. Preprint at https://arxiv.org/ abs/1904.05806 (2019).
- [46] Walck, C. Hand-book on Statistical Distributions for Experimentalists. Internal Report SUF-PFY/96-01, Univ. of Stockholm (2007).

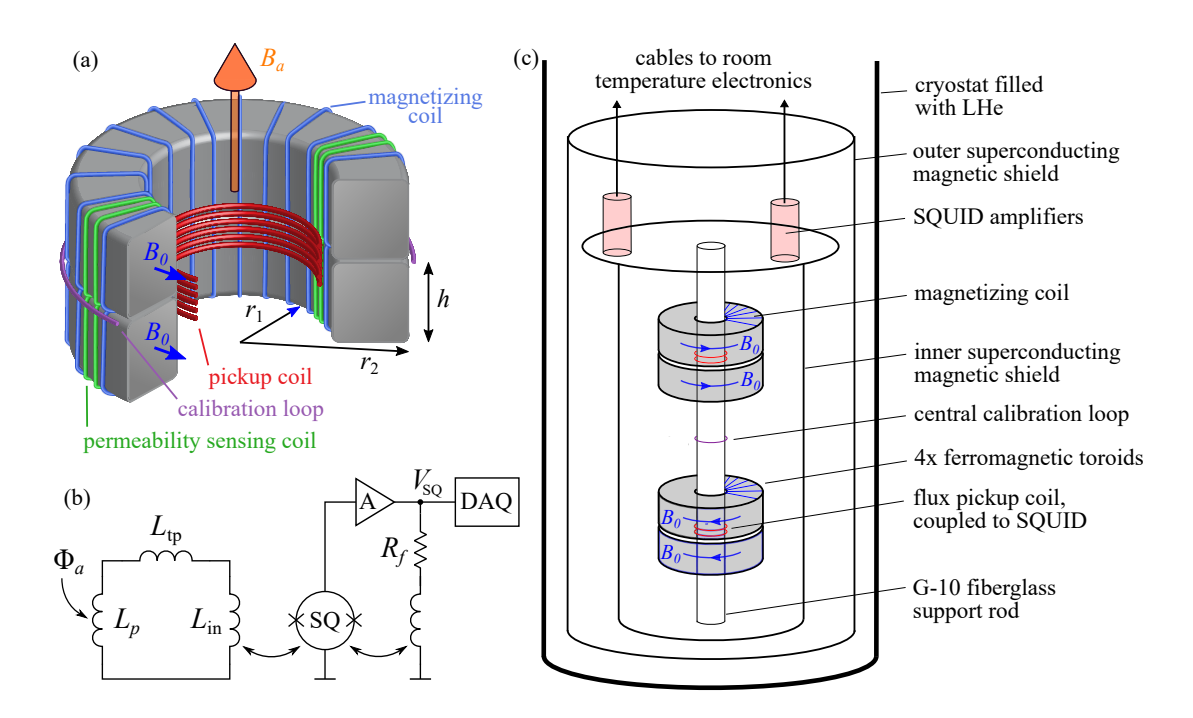


Figure 1: Experimental setup. (a) Schematic of a single detection channel. Two permeable toroids were independently magnetized by injecting current into a magnetizing coil wrapped around each toroid, creating azimuthal field B_0 within each toroid. The electromagnetic coupling $g_{a\gamma}$ of axion-like dark matter induces an oscillating magnetic field B_a , which produces a magnetic flux Φ_a through the pickup coil mounted at the inner circumference of the toroids. Toroid magnetization was monitored by measuring the inductance of the permeability sensing coils. Dimensions: $r_1 = 24.4$ mm, $r_2 = 39.1$ mm, h = 16.2 mm. (b) The circuit model that shows the axion-induced flux Φ_a coupling into the pickup coil (inductance L_p). The pickup coil was coupled to the SQUID magnetic flux sensor (SQ) via twisted pair leads (inductance $L_{\rm tp}$) and input coil (inductance $L_{\rm in}$). The SQUID was operated in the flux-locked-loop mode, using amplifier A and feedback resistance R_f . The feedback voltage $V_{\rm SQ}$ was digitized and recorded by the data acquisition system (DAQ). (c) The SHAFT experimental schematic. The apparatus contained four permeable toroids, shown magnetized in the (++, --) configuration, which was used to collect data sensitive to axion-like dark matter. The experiment operated at 4.2 K in a liquid helium bath cryostat.

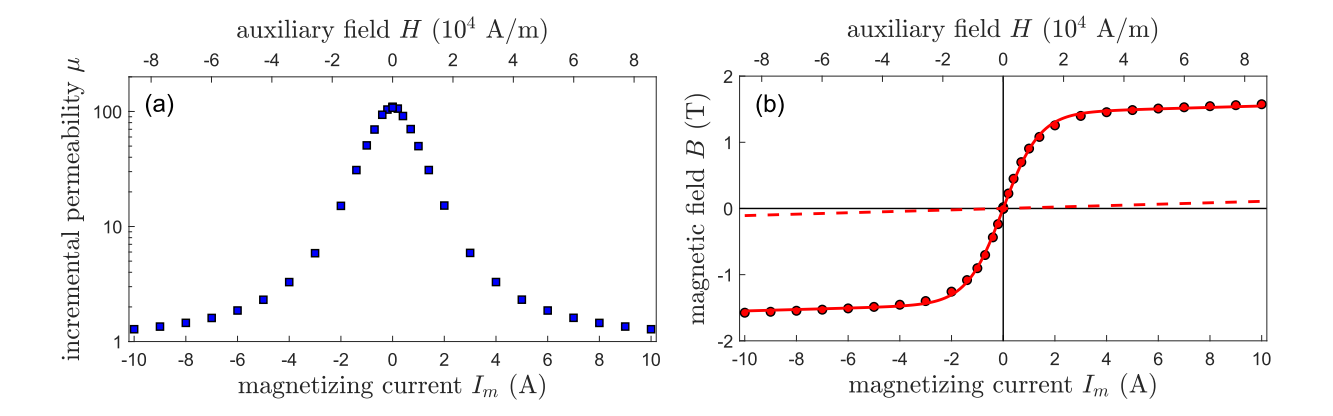


Figure 2: Toroid magnetic properties. (a) Measurements of the toroid incremental permeability at temperature 4.2 K, for currents up to 10 A injected into the magnetizing coil. Incremental permeability decreases with increasing current, as the magnetic material saturates. (b) The azimuthal magnetic field B_0 inside the toroid, calculated by integrating the incremental permeability data. Solid line shows the saturation model: $B = \mu_0 \left[H + M_0 \tanh(H/H_0) \right]$, with best-fit saturation magnetization $M_0 = (1.15 \pm 0.03) \times 10^6$ A/m and saturation field $H_0 = (1.20 \pm 0.05) \times 10^4$ A/m (Supplementary Information). Dashed line shows the magnetic field that would be created inside an air-core toroid. One standard deviation error bars are on the order of symbol size for both panels.

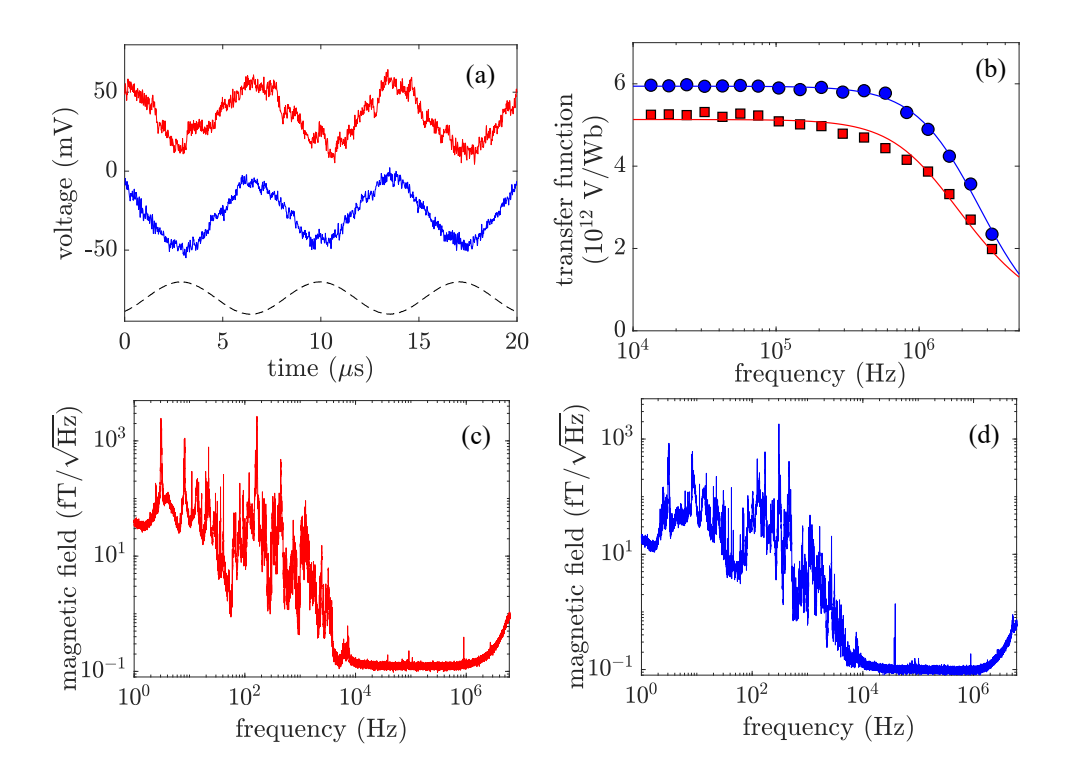


Figure 3: Calibration and sensitivity of SQUID detection channels. (a) Magnetic flux calibration measurements: sinusoidally-varying current was injected into the central calibration loop and the response of the two SQUID detection channels was recorded. Dashed black line shows the signal proportional to injected current at 142 kHz; red and blue lines show the time-domain response of channels A and B, respectively (offset along the y-axis for clarity). At this frequency, the channels are in phase. The full quadrature calibration was performed as a function of excitation frequency up to 4 MHz (Supplementary Information). (b) The frequency dependence of the absolute value of SQUID flux-to-voltage transfer function for channel A (red squares) and channel B (blue circles). The low-frequency value of the transfer function was consistent with the inductive coupling model shown in fig. 1(b), and the high-frequency roll-off was due to the finite bandwidth of the SQUID flux-locked loop feedback electronics. One standard deviation error bars are on the order of symbol size. (c,d) SQUID magnetic sensor noise spectra for channels A and B, respectively. Noise at frequencies below 10 kHz was correlated with cryostat vibrations, and the degradation at frequencies above 1 MHz was due to SQUID transfer function roll-off.

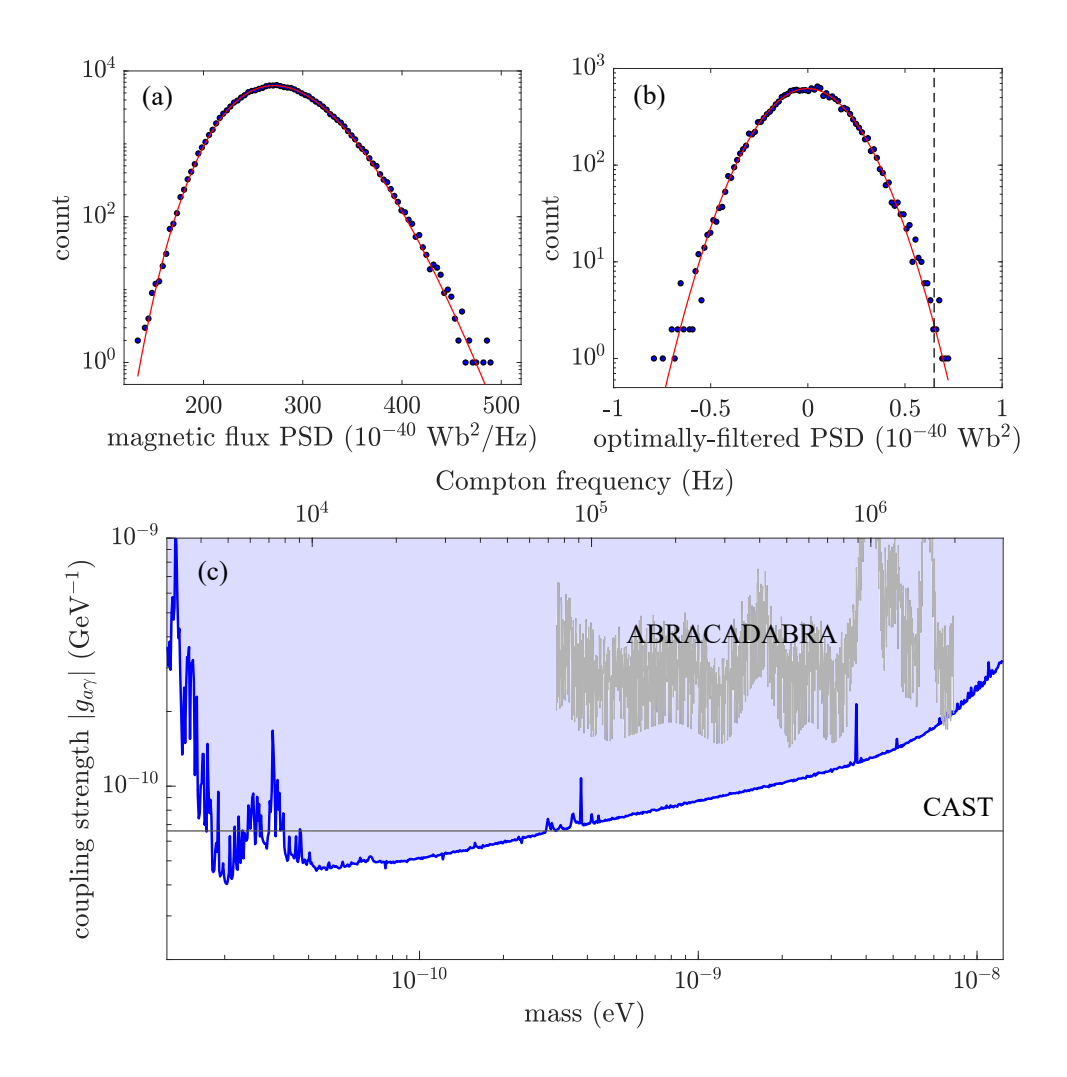


Figure 4: Results of axion-like dark matter search. (a) The histogram of the magnetic flux power spectral density data within a frequency bin centered at the frequency $\nu_b = 10.04$ kHz and with the width $10^4 \beta^2 \nu_b \approx 0.08$ kHz. The histogram is consistent with a chi-square distribution with 94 degrees of freedom (red line). This distribution is expected because the PSD is formed by adding the squares of the real and imaginary parts of the Fourier transform and averaging over 47 data blocks. Therefore, it is a sum of squares of 94 independent normally-distributed random variables [46]. (b) The histogram of data in the $\nu_b = 10.04$ kHz bin, optimally-filtered by convolving with the standard halo model axion-like dark matter signal spectral shape. The red line shows the normal distribution fit, and the dashed vertical line shows the 3.355 σ threshold for flagging candidate frequencies. (c) Limits on the electromagnetic coupling strength of axion-like dark matter in the mass range from 12 peV to 12 neV. The blue shaded region is excluded by our data at 95% confidence level. The horizontal black line shows the limit from the CAST helioscope [22], and the grey line shows the ABRACADABRA limits on axion-like dark matter [35]. The trend of improved sensitivity to $g_{a\gamma}$ at lower ALP masses (frequencies) is due to narrowing linewidth of the ALP signal, which scales as $\beta^2 \nu_a \approx 10^{-6} \nu_a$ in the standard halo model.